© 2014. Published by The Company of Biologists Ltd | Journal of Cell Science (2014) 127, 124–136 doi:10.1242/jcs.133272

RESEARCH ARTICLE

Entry into the nuclear pore complex is controlled by a cytoplasmic exclusion zone containing dynamic GLFG-repeat nucleoporin domains

Jindriska Fiserova[1], Matthew Spink[1], Shane A. Richards[1], Christopher Saunter[2] and Martin W. Goldberg[1,*]

ABSTRACT

Nuclear pore complexes (NPCs) mediate nucleocytoplasmic movement. The central channel contains proteins with phenylalanine-glycine (FG) repeats, or variations (GLFG, glycine-leucine-phenylalanine-glycine). These are 'intrinsically disordered' and often represent weak interaction sites that become ordered upon interaction. We investigated this possibility during nuclear transport. Using electron microscopy of *S. cerevisiae*, we show that NPC cytoplasmic filaments form a dome-shaped structure enclosing GLFG domains. GLFG domains extend out of this structure and are part of an 'exclusion zone' that might act as a partial barrier to entry of transport-inert proteins. The anchor domain of a GLFG nucleoporin locates exclusively to the central channel. By contrast, the localisation of the GLFG domains varied between NPCs and could be cytoplasmic, central or nucleoplasmic and could stretch up to 80 nm. These results suggest a dynamic exchange between ordered and disordered states. In contrast to diffusion through the NPC, transport cargoes passed through the exclusion zone and accumulated near the central plane. We also show that movement of cargo through the NPC is accompanied by relocation of GLFG domains, suggesting that binding, restructuring and movement of these domains could be part of the translocation mechanism.

KEY WORDS: Nuclear pore, Transport, Phenylalanine-glycine repeat, GLFG

INTRODUCTION

Nucleocytoplasmic transport is mediated by the nuclear pore complex (NPC), which provides a selectively gated conduit for soluble and membrane proteins (Fernandez-Martinez and Rout, 2012; Zuleger et al., 2012), and other molecules. It consists of proteins that anchor it to the pore membrane, remarkably stable 'scaffolding' proteins (Savas et al., 2012) and nucleoporins containing phenylalanine-glycine (FG) repeats. Some contain the simplest FG-repeat, others are more complex, like GLFG (Gly-Leu-Phe-Gly). Intervening sequences can be relatively charged or more hydrophobic (Yamada et al., 2010), affecting *in vitro* structures and properties. FxFG domains have higher charge content and are extended, whereas GLFG domains are less charged and more folded.

NPCs have a series of concentric rings (Goldberg and Allen, 1995). In the centre is the 'spoke ring complex' (Akey and Radermacher, 1993) consisting of scaffolding nucleoporins and membrane proteins (Bilokapic and Schwartz, 2012; Hoelz et al., 2011). There is a ring on the cytoplasmic face, consisting of a 'star'-shaped ring in the membrane, with a thin ring on top, then eight bipartite subunits (Goldberg and Allen, 1995). Rod-shaped particles extend into the cytoplasm.

Vertebrate cytoplasmic filaments contain Nup358 (Wu et al., 1995; Walther et al., 2002), an FG nucleoporin that binds Ran and RanGAP1 through an SUMO modification (Lee et al., 1998; Matunis et al., 1998). Yeast do not have Nup358, but possess cytoplasmic filaments (Kiseleva et al., 2004).

FG domains are intrinsically disordered (Denning et al., 2003; Patel et al., 2007), suggesting several types of model for their roles in transport (Wälde and Kehlenbach, 2010). In one, FG domains interact with each other hydrophobically, forming a 'hydrogel' (Ribbeck and Görlich, 2001), whereas in another they do not interact and instead constitute a cloud that occludes the NPC entrance (Rout et al., 2000). In the former model, nuclear transport factors (karyopherins) gain access to the channel by utilising hydrophobic surface domains that can integrate into the hydrogel through hydrophobic interactions (reviewed by Cook et al., 2007). In the latter model, the energy barrier that prevents entry into the crowded, small dimensions of the channel is overcome by transient binding of the karyopherins to the FG domains (Rout et al., 2000). In both models, FG domains play a passive barrier role that must be broken to allow transport. Lim et al. (Lim et al., 2007) have shown that the FG domain of Nup153 is present in different positions, but, in the presence of excess karyopherin, it retracts towards the centre. This is reversed by binding of RanGTP which dissociates karyopherins from FG domains. Nup153 FG domains (Lim et al., 2007) exist in an extended 'brush boarder' conformation, except in the presence of karyopherin β, when they collapse into folded conformations. Restructuring is reversed by RanGTP, suggesting that folding and unfolding in response to binding and release of karyopherins could be central to nuclear transport.

Because most information on FG domain dynamics is based on *in vitro* experiments or isolated nuclear envelopes, we wanted to investigate FG domain dynamics *in vivo*. We looked at the conformation of GLFG domains in budding yeast using high-pressure freezing (HPF) and low-temperature embedding for optimal preservation of ultrastructure, and to capture intermediates in the rapid nuclear transport process. We show that GLFG distribution varies between NPCs and that variation could be related to import steps.

[1]School of Biological and Biomedical Sciences, Durham University, Science Laboratories, South Road, Durham DH1 3LE, UK. [2]Department of Physics, Durham University, Science Laboratories, South Road, Durham DH1 3LE, UK.

*Author for correspondence (m.w.goldberg@durham.ac.uk)

Received 16 April 2013; Accepted 29 September 2013

Journal of Cell Science

Journal of Cell Science (2014) 127, 124–136 doi:10.1242/jcs.133272

RESULTS

Yeast cytoplasmic filaments form a basket-like structure

We modified a previous procedure to study yeast NPCs by field emission scanning electron microscopy (feSEM) (Kiseleva et al., 2004), leaving ribosomes in place (Fig. 1A). Although difficult to see, NPCs are well preserved (Fig. 1B; Fig 1D–H) and have cytoplasmic filaments, extending towards the centre of the NPC forming a basket-like structure.

Evidence for cytoplasmic filaments is seen in transmission electron microscopy (TEM) of high pressure frozen cells (Fig. 1C, contrast reversed; dense material is white, in Fig. 1C′, membrane and filaments are traced white). In feSEM the filaments have a diameter of 8–9 nm, whereas in TEM they measure ~6 nm, which can be accounted by the chromium coat in feSEM.

Although cytoplasmic filaments are thought of as eight separate filaments, connections between them (forming a basket-like structure) have been observed by cryo-electron microscopy (detergent-extracted nuclear envelopes, see figure 9a in Akey and Radermacher, 1993) and cryo-feSEM (Fig. 1I).

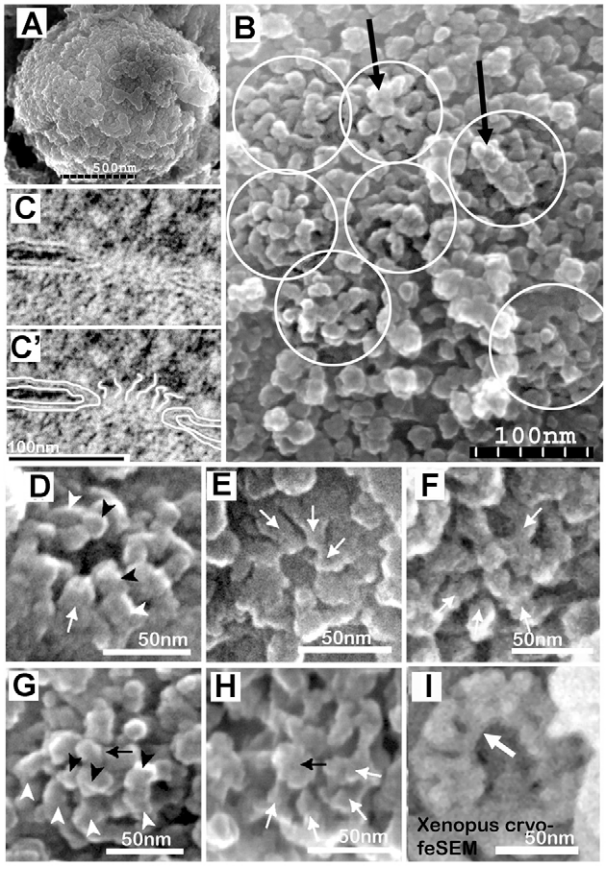

Fig. 1. Yeast NPC cytoplasmic filaments form a basket-like structure. FeSEM image of isolated *S. cereviseae* nucleus at low magnification (A) and high magnification (B), showing NPCs (circled) surrounded by ribosomes. (C,C′) Cytoplasmic filaments are shown in cross sections through the nuclear envelope by TEM. (D–H) Details of cytoplasmic filaments (white arrows) are shown. The cytoplasmic filaments are often bipartite with a component attached to the cytoplasmic ring (white arrowheads) and a distal component, which could be responsible for joining adjacent filaments (black arrowheads). Some NPCs appear empty in the centre (D,E), whereas others have dense material protruding from the cytoplasmic basket-like structure (B,G,H, black arrows). (I) Cryo-feSEM image of *Xenopus* oocyte NPC.

Such a conformation could also be induced in *Xenopus* oocytes by excess RanGTP (Goldberg et al., 2000).

Dome-shaped 'exclusion zone'

Cyto-filaments could contain FG domains. Because FG domains might be involved in weak interactions, with each other (Patel and Rexach, 2008) and with karyopherins (Rexach and Blobel, 1995), it is possible that interactions are altered during isolation of nuclei. We were therefore interested in the conformation of FG domains *in situ*. Optimal, rapid fixation of yeast NPCs is achieved by HPF, followed by low-temperature fixation and embedding (freeze substitution, FS) (Fiserova and Goldberg, 2010). This enables us to catch transient interactions and maintain fragile structures.

HPF/FS thin sections show two leaflets of each nuclear membrane (Fig. 1C; Fig. 2A) and we can follow the membrane path (Fig. 2A–E) and can delineate the 'pore'. On the cytoplasmic face, there is a 'zone of exclusion' where ribosomes and other components are absent (Fig. 2). This has two components: a dense region that is within the pore and forms a 'dome' in the cytoplasm (Fig. 2, white dotted line); and a less dense region that extends further (Fig. 2, black dotted line).

The inner region extends 15–30 nm from the central plane. In comparison, cytoplasmic filaments seen by feSEM are ~30 nm in length, and so could maximally extend ~45 nm from the central plane of the NPC (the filament length plus half the depth of the yeast NPC, if oriented perpendicular to the plane). However, they were angled towards the centre, so would not extend this far out. Therefore, we propose the dense zone is contained within the cytoplasmic basket-like structure.

We measured the 'height' of the exclusion zone (the perpendicular distance between the central plane of the NPC and the most distal extent of the exclusion zone. The average height was 48 nm (median, 46 nm; s.d., 13 nm; $n=49$), ranging ~30 nm–~90 nm.

FeSEM revealed some NPCs have a dome of filaments (e.g. Fig. 1D, white arrow), which could correspond to the heavily stained dome seen by TEM (Fig. 2), whereas others have material extending from the dome (Fig. 1G,H, black arrows), which can be extensive (Fig. 1B, large black arrows) and could correspond to the less-stained exclusion zone (Fig. 2A′–E′, black dotted lines).

The C-terminal anchor of Nup116 lines the NPC channel

The cytoplasmic filaments have a defined structure, whereas material in the centre appears amorphous. Intrinsically disordered FG domains (Denning et al., 2003) would be consistent with amorphous structures. We therefore wanted to determine where FG domains locate. We used domain-specific antibodies to the C-terminal anchor of Nup116p, and to the GLFG domain. The position of the C-terminal anchor is shown in Fig. 3A–D. Because the membrane is difficult to see after labelling, it is traced for clarity (Fig. 3A′–D′). There is inherent imprecision of labelling in electron microscopy that will vary from 0–15 nm (Murphy et al., 1988; Ban et al., 1994; Iborra and Cook, 1998), but these images show that the Nup116p C-terminal anchor is close to the NPC central plane. The labels were almost always close to the pore membrane, suggesting that the C-terminal domain of Nup116p is located around the walls, within the channel. Consistent with previous studies (Rout et al., 2000), we found a bias towards the cytoplasmic side (53% on the cytoplasmic side compared to 47% on the nucleoplasmic side, $n=166$ accumulated data from three separate experiments).

Journal of Cell Science (2014) 127, 124–136 doi:10.1242/jcs.133272

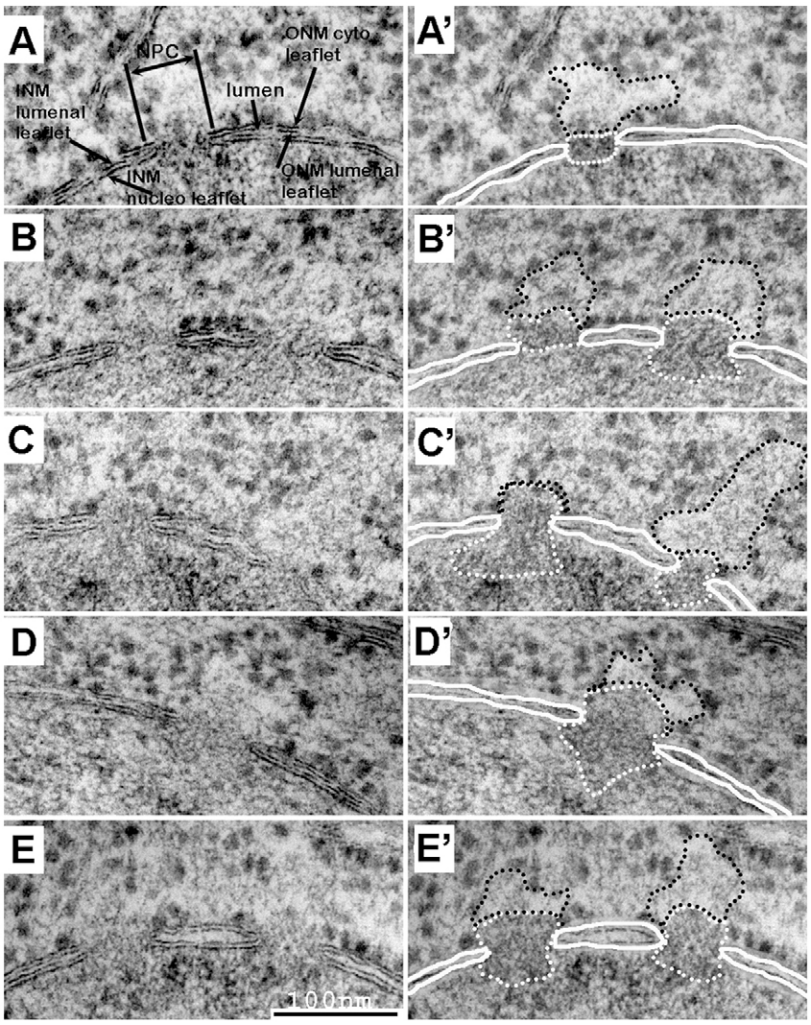

Fig. 2. Exclusion zone on cytoplasmic face of yeast NPC. TEM thin sections of HPF/FS yeast cells, showing inner, outer and pore membranes, the dense region (area delineated by white dotted line) within the pore and the zone of exclusion (area delineated by black dotted line).

Previous feSEM (Ho et al., 2000) has shown that the same antibody labelled around the NPC periphery close to the membrane. The same study provided full characterisation of this antibody (WU600), including the labelling a single band of ~120 kDa on western blots.

GLFG domains extend away from the NPC channel and their localisation varies between NPCs

We labelled sections with a previously characterised antibody raised against the N-terminal GLFG domain of Nup116p (WU956; Bucci and Wente, 1998; Strawn et al., 2004). On western blots (Fig. 3L), this antibody labels a band of ~120 kDa, and other minor bands. When the GLFG domain of Nup116p is deleted, the ~120 kDa band disappears, indicating the antibody predominantly labels the GLFG domain of Nup116p. Several minor bands also disappear which could represent degraded Nup116p or possibly, splice variants. In the Nup116 GLFG deletion strain, three bands remain, suggesting that the antibody also binds to other proteins. One band runs at ~55 kDa, and could represent Nup57p, also a GLFG nucleoporin. To test this we looked at a strain where the GLFG domain of Nup57p had been deleted. The ~55 kDa band disappeared. To confirm this we looked at another strain where the Nup57p gene was tagged with GPF and the ~55 kDa band disappeared and an additional higher molecular mass band appeared. Therefore we can conclude that the antibody labels Nup57p specifically on the GLFG domain. Another band, at ~100 kDa, was similarly shown to be Nup100p, also a GLFG nucleoporin. We also find that in a strain containing Nup49p fused to a TAP tag, the ~45 kDa band disappears, with a new band appearing at ~70 kDa (supplementary material Fig. S1), suggesting that the antibody labels Nup49p. Likewise a Protein A tag on Nup116p results in increased molecular mass. We therefore conclude that the antibody labels GLFG domains.

The anti-GLFG antibody gave a strikingly different localisation to the antibody against the C-terminus of Nup116p (Fig. 3E–G). Whereas the C-terminus was at the edge of the channel, the GLFG domain could be anywhere within the channel (Fig. 3E–G). It also extended up to ~80 nm from the central plane, into the cytoplasm or nucleoplasm. This is further than the extent of the cytoplasmic filaments or nuclear baskets (Goldberg and Allen, 1992; Kiseleva et al., 2004). Some NPCs have cytoplasmic GLFG labelling (Fig. 3E,E′), some have a symmetrical labelling distribution (Fig. 3F,F′), and some have nucleoplasmic labelling (Fig. 3G,G′). Because the anti-Nup116p GLFG antibody recognises other GLFG nucleoporins, we compared the labelling of two mutants where the GLFG domains of Nup57p (Fig. 3H,H′,I,I′) or Nup116p (Fig. 3J,J′,K,K′) had been deleted, in addition to the localisation of asymmetric Nup FG domains (Strawn et al., 2004). We detected little difference in the distribution of labels between the wild-type

Journal of Cell Science (2014) 127, 124–136 doi:10.1242/jcs.133272

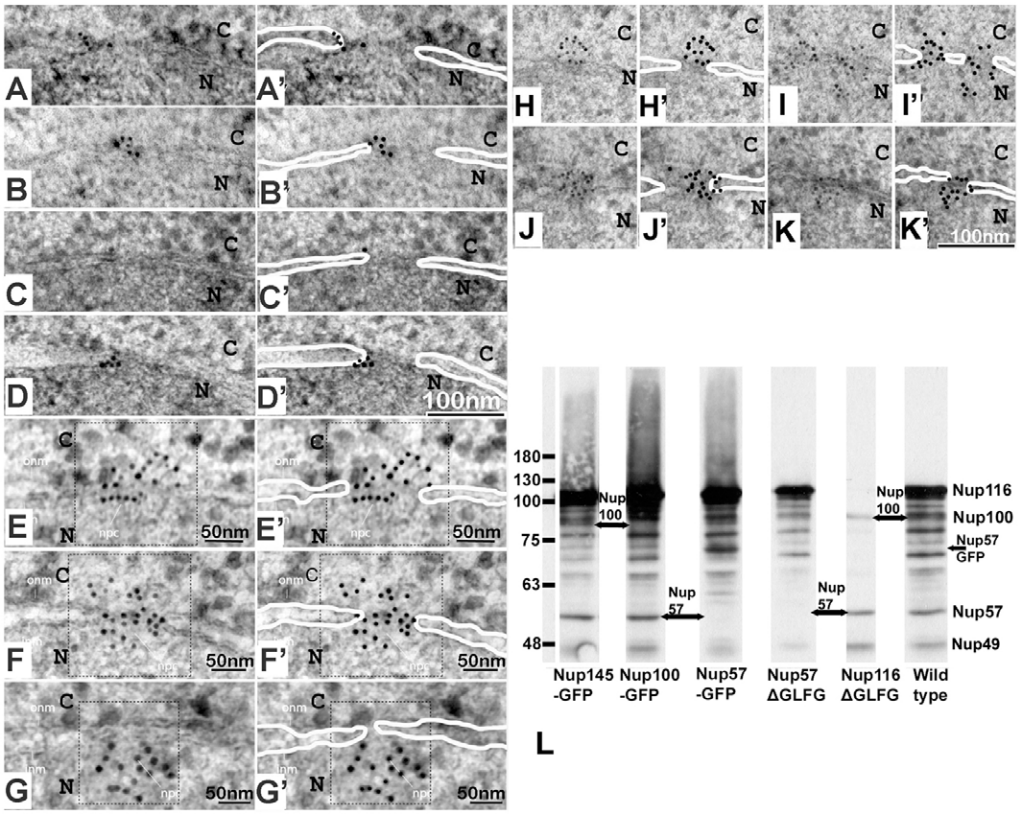

Fig. 3. GLFG domains of Nup116p extend away from the C-terminal anchor. (A–D) Immunogold labelling of HPF/FS thin sections with an antibody against the Nup116p C-terminal globular anchor domain. The membrane is traced for clarity (A′–D′). Anti Nup116p GLFG domain labelling shows cytoplasmic (E,E′), central (F,F′) and nuclear (G,G′) distributions of the GFLG domains, which appear similar in mutants where the GLFG domains of either Nup57 (H,H′,I,I′) or Nup116 (J,J′,K′K′) have been deleted. N, nucleus; C, cytoplasm. (L) Western blot of whole cell lysates of wild-type, deletion mutant and tagged Nup strains as indicated. Sizes of molecular mass markers (Abcam Prism Ultra Protein Ladder) are shown on the right.

and either deletion mutant, suggesting the antibody labels GLFG domains of both Nup116p and Nup57p, and that the GLFG domains of these two proteins have similar locations.

The position of the GLFG domains within the exclusion zone varies

We looked for correlations between GLFG labelling and the exclusion zone. Some NPCs (Fig. 4A) showed a strong correlation, although generally the exclusion zone extended further than GLFG labelling. When GLFG labelling was symmetrical or nucleoplasmic, there was a pronounced cytoplasmic exclusion zone (Fig. 4) that lacked GLFG labelling (Fig. 4B). This suggests that, although the GLFG domains extend into the exclusion zone, the zone can maintain its exclusion properties when the GLFG domains are not within it.

We quantified how far the GLFG labelling extended into the cytoplasm giving an average of 35 nm (median, 35 nm; s.d., 12; $n=94$). This was a little less than the exclusion zone. However, whereas the exclusion zone was always at least ~30 nm, and up to ~90 nm, into the cytoplasm, the GLFG labelling sometimes barely extended into the cytoplasm at all and did not usually extend as far. Therefore GLFG domains could be completely within the pore, or be present up to the extent of the zone. Therefore other protein structures (such as the cytoplasmic filaments) or possibly FG domains from other nucleoporins, must also constitute the exclusion zone and be extended when GLFG domains are within the central channel or within the nucleoplasm.

Relationship between the exclusion zone and the cytoplasmic basket-like structure

Nuclei were immunogold labelled with anti-GLFG antibody and viewed using scanning electron microscopy (SEM). NPCs were difficult to see but we could detect cytoplasmic filaments (Fig. 5A, arrows) and immunogold labelling appeared clustered, which is consistent with the TEM results (Figs 3, 4). Clustering is clear when the backscatter image is viewed without the secondary electron image (Fig. 5B). This is clearer when the dots are extracted from the background (Fig. 5C).

To confirm clustering, we determined the coordinates of each gold particle and performed a nearest neighbour analysis, presented as a frequency distribution (Fig. 5D), the results are typical of clustering, giving a mean nearest neighbour distance of 16.1±3.4 nm (s.e.m.). We used another morphometric program, PAST (Hammer et al., 2001), which, with edge correction, gave a nearest neighbour distance of 15.8 nm compared to an expected distance for a random (Poisson) distribution of 20.2 nm ($P<0.001$). The R value (probability that the distribution is random) was 0.78 (for random distributions $R=1$, over-dispersion $R>1$, clustering indicated by values <1). Ripley's K analysis, indicates clustering because almost all the values are >0 (Fig. 5E). Therefore the clustered labelling indicated the position of NPCs and organisation of GLFG domains.

Where the NPCs were clear (Fig. 5F–H), labelling appeared less clustered, in contrast to the clear clusters in less-easily imaged NPCs (Fig. 5I–K). It can be seen that the latter (Fig. 5I–K) have a dense mass enclosed by filaments (Fig. 5K, black arrows). Although the gold particles are easy to detect in the backscatter image, the gold-particle–antibody complex is not usually visible in the secondary electron image. An explanation for this is that strongly backscattering gold particles are just beneath the surface being imaged and are not generating secondary electrons. Therefore the cytoplasmic filaments, which are imaged directly by secondary electrons, enclose the GLFG domains, which are detected by electrons backscattered from the

Journal of Cell Science (2014) 127, 124–136 doi:10.1242/jcs.133272

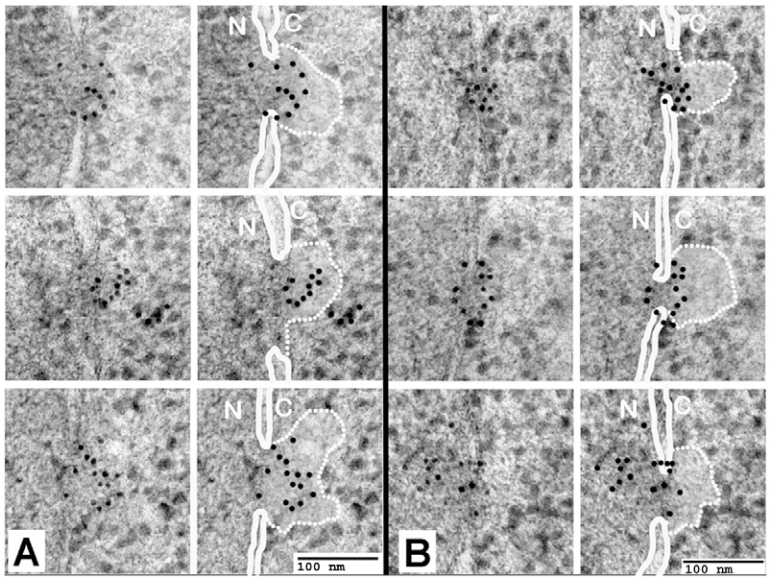

Fig. 4. The exclusion zone may or may not contain GLFG domains. Location of GLFG labelling correlated with zone of exclusion, showing that although GLFGs can be throughout the zone of exclusion (A), the zone is still present when the GLFGs are located within the NPC channel or on the nucleoplasmic side (B). Left-hand images are the raw data, right-hand images show the zone of exclusion delineated by the white dotted line and the gold particles marked with a black dot. N, nucleus; C, cytoplasm.

immunogold particles. This is consistent with TEM observations, where we see an exclusion zone, which can be defined by the cytoplasmic filaments, and a central mass containing GLFG domains. In the TEM, we see GLFG domains and/or exclusion zones extending some distance into the cytoplasm in some NPCs and retracted into the channel in others. Likewise in the SEM image we see GLFG labelling in extended masses in the NPC centre in some NPCs (Fig. 5I–K) and more dispersed GLFG labelling and correspondingly little central mass in others (Fig. 5F–H).

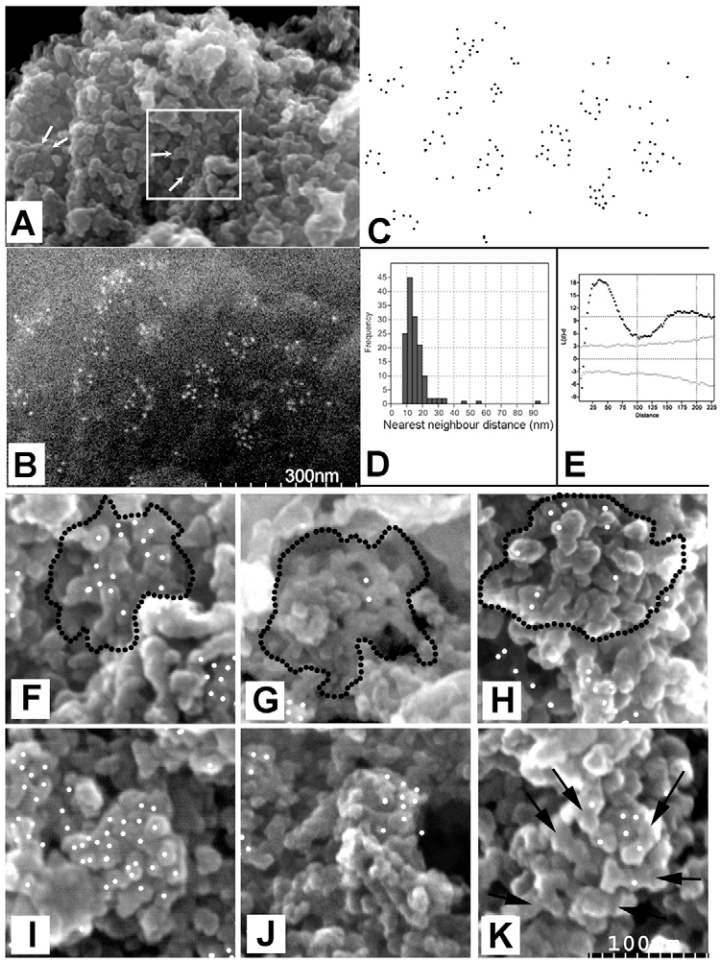

Fig. 5. Clustering of GLFG domains. FeSEM of anti-GLFG immunogold labelling, showing secondary electron image (A) with visible cytoplasmic filaments (arrows), and the backscatter image (B) showing position of 10-nm gold particles. Gold particle positions were extracted (C), showing clustering. This was used for the nearest neighbour analysis (D), Ripley's *K* cluster analysis (E) (where the grey dots represent the 95% confidence limits for computed random distribution and black dots represent data). (F–K) FeSEM of anti-GLFG immunogold labelling. In some NPCs, cytoplasmic filaments are visible but gold particles within appear less clustered (F–H), whereas in others (I–K) labels are clustered and details of the cytoplasmic filaments are difficult to resolve.

Journal of Cell Science (2014) 127, 124–136 doi:10.1242/jcs.133272

GLFG domains are concentrated within the central channel, biased to the cytoplasmic side, and extend into the cytoplasm or nucleus

We developed a program to analyse TEM images (Delineator) that determines the coordinates of gold labels with respect to the central plane. This allowed us to analyse large numbers of images, giving us a picture of how the GLFG domains are distributed throughout an average NPC. Fig. 6A shows a frequency distribution of labels for wild-type cells superimposed onto an NPC at the same scale. The median distance from the central plain is +6 nm, with a standard deviation of ~20 nm. This means there is a skew of GLFG domains (Fig. 6A, arrow) towards the cytoplasm and the majority are located within about 30 nm of the central plane on the cytoplasmic side and 10 nm on the nucleoplasmic side. However, the labelling could extend considerably further: up to ~80 nm on either side.

Because the C-terminal anchor domain is always within the channel, the GLFG domains presumably adopt a number of different conformations. They must be either highly extended, or more compact. Looking only at labels on one side of the central plane, we find that the median distance is 16.5±13 nm (s.d.) for the cytoplasmic side and 10±10 nm (s.d.) for the nucleoplasmic side. ~80% of the GLFG domain mass is confined to a 40-nm-deep region in the central channel from 10 nm on the nucleoplasmic side to 30 nm on the cytoplasmic side.

Fig. 6B shows accumulated coordinates of gold particles superimposed on a tracing of the membranes from the same image, only using images of NPCs that were cut though the centre. The depth of the channel is about 30 nm (Yang et al., 1998) and is symmetrical about the central plane. The GLFG domains of highest density fill the channel, protruding beyond the cytoplasmic ring on the cytoplasmic side, but not on the nucleoplasmic side, although some GLFG domains extend further on either side. A kernel density analysis (Fig. 6C) indicates that on average the GLFG domains are more tightly packed on the nucleoplasmic side.

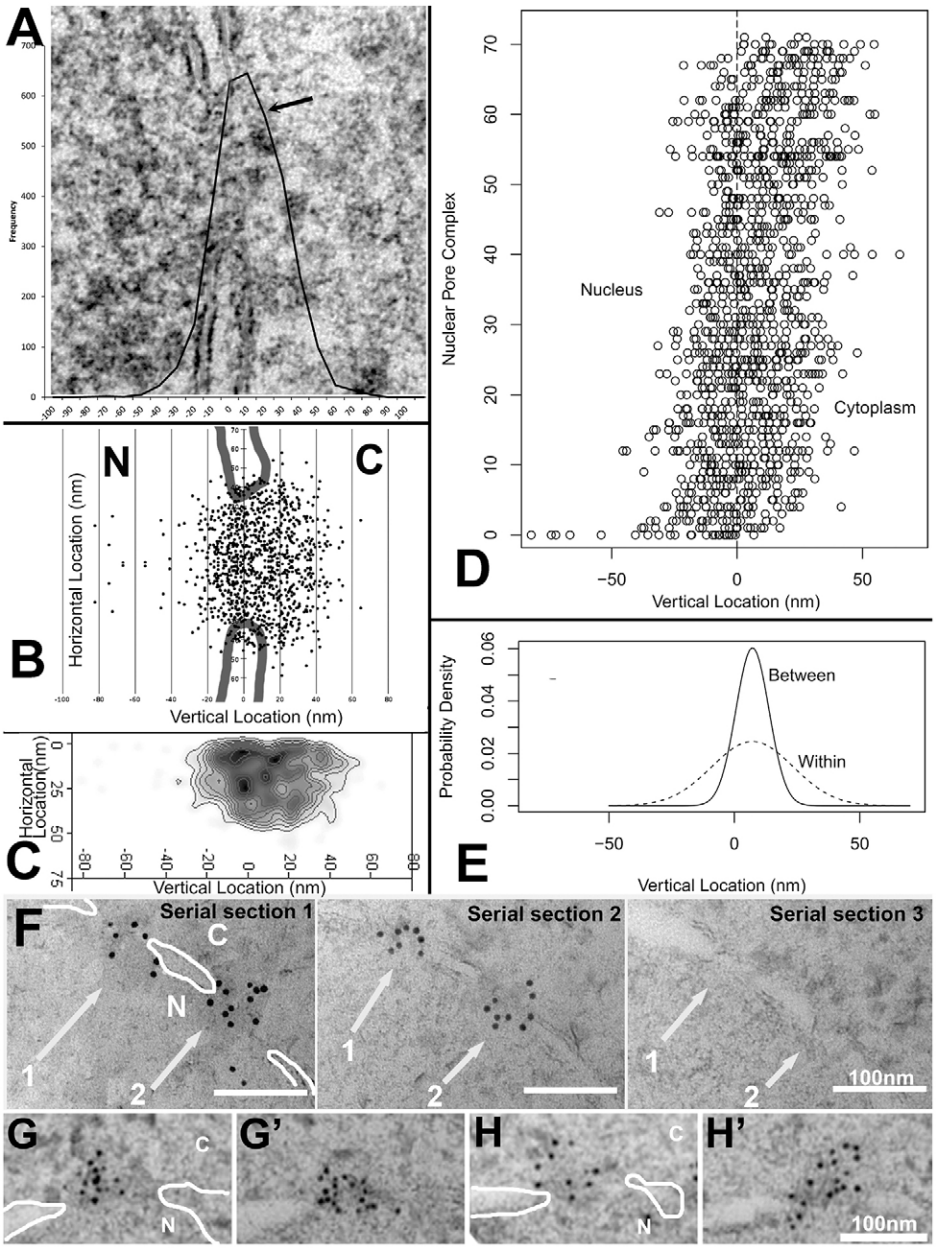

Fig. 6. Most GLFGs are concentrated in the central channel. Quantification of the immunogold labelling with anti-GLFG antibody. (A) Frequency distribution of labels related to the central plane of an average NPC, superimposed on the image of a typical cross-section. The arrow indicates the shoulder, showing skewing to the cytoplasm. (B) Accumulated coordinates of 544 gold particles from 72 NPCs superimposed on same image as that shown in A (there are 1088 dots shown because coordinates are measured as a distance from central plane vs central axis and cannot distinguish which side of the axis they are on, so we produced a mirror image). A density analysis is shown in the contour map (C). (D) Vertical distribution of gold particles from 72 NPCs. NPCs are ordered according to the mean position of the gold particles. (E) Best-fit normal distributions describing variation in mean vertical location of particles between NPCs (solid line) and variation within all NPCs (dashed line). Analysis showed no clear relation between the variation and mean (i.e. the variation of particles within each NPC is the same for all NPCs). (F) Three consecutive serial sections of the same two NPCs labelled with anti-GLFG antibody showing centrally located GLFG labelling. The position of each NPC is marked by an arrow. The position of membranes is delineated by white line in first section. (G,G′) Two serial sections of the same NPC showing cytoplasmically biased GLFG labelling. (H,H′) An example of extended GLFG labelling of two consecutive sections of same NPC. N, nucleus; C, cytoplasm.

NPCs can be categorised based on the location of GLFG domains

Because we observed that NPCs could have GLFG domains located in different regions we sought to quantify whether this was significant. We did a subjective analysis where NPCs were categorised into whether they had mostly cytoplasmic, symmetrical or nucleoplasmic anti-GLFG labelling. 55% were mostly cytoplasmic, 38% symmetrical and 7% nucleoplasmic ($n=152$). We looked at the number of gold labels in each of the locations and categorised these (the central channel is defined as 9.5 nm from either side of the central plane, gold particles beyond this on either side are defined as cytoplasmic or nucleoplasmic). We found that 49% of gold particles were cytoplasmic, 30.5% were central and 20.5% were nucleoplasmic ($n=1332$).

Although we detected this asymmetric distribution and variation between NPCs, there are several possible functional interpretations. One hypothesis is that GLFG domains that extend some distance into the cytoplasm are highly disordered, then become ordered and retract into the central channel upon interaction with a transport complex. Nucleoplasmically oriented GLFG domains then might represent a release phase of the process. If so, this raises the question about whether the retraction is a coordinated mass movement of GLFG domains into the channel or whether GLFG domains react individually.

We analysed 72 NPCs that were sectioned through the central plane and plotted the z coordinate (distance from the central plane) of each gold label within each NPC (Fig. 6D). NPCs were ordered on the plot according to the size of the mean distance of their gold particles from the central plane. Fig. 6D shows that NPCs can be classified with respect to the position of GLFG domains, but that the variation from one extreme to the other is gradual. It is possible that this variation represents a sampling effect determined by the angle of the section through any particular NPC. A section might only contain the cytoplasmic side of an NPC and not sample the nucleoplasmic side. However in such 'grazing' sections the membranes become indistinct and were therefore not included in the analysis. We also checked for such a sampling bias by carrying out serial section anti-GLFG immunogold TEM (Fig. 6F) and found that the orientation of the labelling was the same from one section to the next in any one NPC. Typically one NPC spanned two sections (which had a nominal thickness of ~25 nm) and in all cases we found that any one section was consistent with its serial pair with regard to the orientation of labelling (Fig. 6F). If GLFG domains can retract and extend (evidence below), these results suggest that there was a loose coordination between individual GLFG domains. We therefore sort to verify this conclusion using a model fitting approach.

We observed one unusual NPC where many of its associated particles were located well within the nucleus, further than all other NPCs (Fig. 6D). As including this had a strong influence on our model fits and conclusions, which is undesirable with model fitting, we took the conservative approach and removed it from our analyses. However, this might represent a rare or transient state. We found strong evidence that the mean vertical location of particles varied between NPCs [LRT (Likelihood ratio tests), $G_1=90.7$, $P<0.001$, see Materials and Methods]. We also found strong evidence that the mean particle location, μ, was non-zero (LRT, $G_1=44.2$, $P<0.001$). However, we found no evidence that the variance of particle locations within NPCs had a linear (LRT, $G_1=0.64$, $P=0.42$) or quadratic (LRT, $G_1=0.75$, $P=0.39$) relationship with the NPC mean. Our best-fit model is described by $\{\mu=7.2$ nm, $\sigma_b=6.6$ nm, $\beta_0=16.2$ nm, $\beta_1=\beta_2=0\}$, indicating that the variation within NPCs is over twice as large as the variation between NPCs (Fig. 6E). This fit also predicts that 82.3% of the particles are expected to lie on the cytoplasmic side of the central plane (Fig. 8D). This cytoplasmic skew could reflect the cytoplasmic bias for the anchor domains of Nup116p and Nup100p (Rout et al., 2000 and data above).

If we assume that all NPCs have a similar structure and that each NPC represents a possible state for any NPC, then the strong evidence of between-NPC variation suggests some degree of coordination of movement within an NPC. However, the estimated high within-NPC variation suggests that this coordination is weak. This analysis does support the hypothesis that some GLFG domains relocate from the cytoplasm to the central channel during transport, and some might also relocate into the nucleoplasm. However, within any individual NPC there was no evidence that GLFG domains became concentrated in any specific domain (we did not detect a relation between NPC mean and its variance). The analysis, therefore, did not support the hypothesis that there was a mass coordinated retraction of GLFG domains into the channel. However, it does support the hypothesis that there is a loosely coordinated movement, but that the majority of GLFG domains are located, or spend most of their time, within the central channel on the cytoplasmic side of the central plane.

This analysis, however, does not have a time reference as we looked at randomly sampled snapshots. We therefore carried out double labelling experiments to compare the position of transport substrates (which overall travel in one direction over time) with the position of the GLFG domains. First, however, we sort to characterise the movement of a transport cargo, compared to a protein passively diffusing through the NPC.

Diffusion and transport through the exclusion zone

If there is an exclusion zone, proteins without NLSs should be excluded, or their entry retarded depending on size. Proteins with NLSs should enter easily. To test this, we expressed GFP in cells and prepared them for anti-GFP immunogold TEM (Fig. 7) (Fiserova et al., 2010). GFP is small enough (27 kDa) to slowly diffuse into the NPC but its entry is highly restricted because it does not have an NLS (Mohr et al., 2009). We found GFP labelling within the exclusion zone of some NPCs (Fig. 7A–C; Fig. 7A′–C′), as expected. However, we also noticed that when there was a high concentration of GFP in the cytoplasm (Fig. 7A, arrows), this stopped at the edge of the exclusion zone so that the density of labelling was less within this zone. This gave the appearance of an accumulation of label around the edge of the exclusion zone, and suggested that entry into the NPC is restricted here rather than at the actual channel. This argues in favour of a barrier extending from the NPC (Rout et al., 2000), but does not exclude the possibility that the barrier could constitute a 'hydrogel' (Ribbeck and Görlich, 2001) or a combination of interacting and non-interacting filaments (Yamada et al., 2010). The restriction point appears to be at the edge of the outer exclusion zone (Fig. 2, black dotted line), rather than the inner dense area (Fig. 2, white dotted line). Because feSEM images suggest that the exclusion zone is composed of amorphous material, protruding from the cytoplasmic filaments, we suggest that it is this material that is the barrier into the pore, rather than the cytoplasmic filaments. Furthermore the cytoplasmic filaments are only ~30 nm in length and therefore could not extend as far as the exclusion zone unless they were able to significantly change conformation, for which there is no evidence.

Journal of Cell Science (2014) 127, 124–136 doi:10.1242/jcs.133272

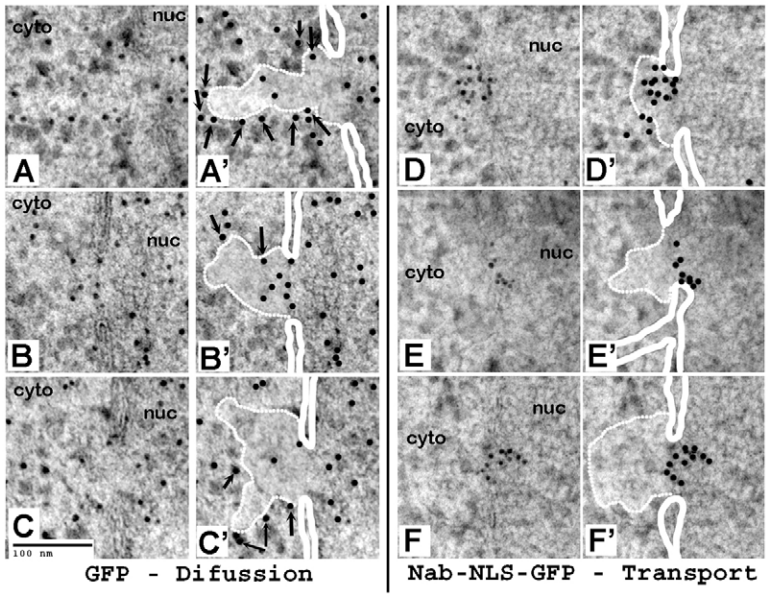

Fig. 7. NLS-containing proteins move rapidly through the exclusion zone. Location of GFP (A–C) compared to NLS-tagged GFP (D–F) using anti-GFP immun-gold labelling, to show the difference between diffusion (GFP) and active transport (NLS–GFP), and how this relates to the extent of exclusion zone. (A′–F′) As A–F, with membranes traced in white, the exclusion zone indicated by the white lines and immunogold particles marked with a black dot. Arrows show gold particles, indicating GFP around the edge of the exclusion zone.

Next, we expressed GFP fused to the Nab2p NLS which is imported via Kap104p. We immunogold-labelled sections with anti-GFP antibody. This gave a strikingly different distribution to that found for GFP without the NLS within the NPC and exclusion zone. There is almost no label around the edge of the exclusion zone and labelling is highly clustered within the channel (Fig. 7E,E′), as well as the cytoplasmic dense zone, which we presume is enclosed by cytoplasmic filaments (Fig. 7D,D′) or the nucleoplasmic dense zone, which we presume is enclosed by the nuclear basket (Fig. 7F,F′). To quantify this, we subjectively judged whether a label was within the dense zone or within the exclusion zone. We estimated that

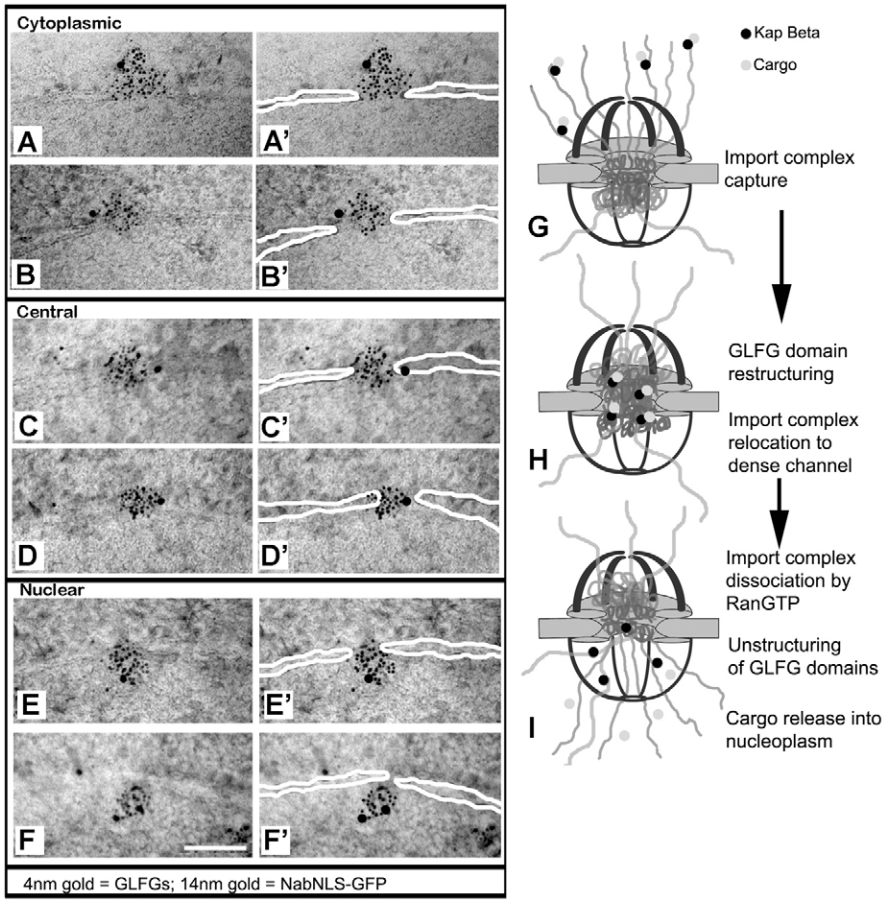

Fig. 8. GLFG domains colocalise with transport cargoes as they move through the NPC. Double immunogold labelling of GLFG domains (small gold particles) and GFP–NLS transport cargo (large gold particles), showing colocalisation in the cytoplasm (A,A′,B,B′), central region of the NPC channel (C,C′,D,D′) and nucleoplasm (E,E′,F,F′). A possible interpretation of these images is presented in G–I.

88% of Nab2p labelling was within the dense zone and 12% was in the exclusion zone (from 25 NPCs, 49 gold particles), whereas, conversely, 31% of GFP alone labelling was in the dense zone and 69% was in the exclusion zone (25 NPCs, 131 gold particles).

One possible interpretation of this data is that import complexes rapidly move through the exclusion zone into the dense zone, before being released into the nucleoplasm. The images also suggest the possibility of a 'pause' within the dense zone, because of the apparent accumulation there. In contrast, diffusing molecules appear to encounter a partial barrier (presumably size dependent) at the exclusion zone, but having entered this zone, they diffuse randomly within it (Fiserova et al., 2010).

Import cargo location correlates with GLFG position

The above results suggest that the location of GLFG domains varies between NPCs (Fig. 4). This suggested that GLFG domains could undergo conformational changes to dynamically move within the NPC and that this movement could be part of transport. Electron microscopy is a static technique and it is not possible to say whether these are dynamic variations. However, we can begin to understand the dynamics by correlating the GLFG location with the location of a molecule that we know interacts with them and moves through the NPC over time in the cytoplasmic to nucleoplasmic direction. We therefore carried out double labelling, looking at the position of import cargo versus GLFG domains. We expressed GFP-conjugated to Nab2p NLS, prepared samples for immuno-EM and labelled them with mouse anti-GFP and rabbit anti-GLFG antibodies, followed by 10-nm-gold-labelled anti-mouse-Ig and Nanogold-labelled (1.4 nm) anti-rabbit-Ig antibodies. The size of the gold particles was then increased to about 14 nm and 4 nm, respectively, as indicated in the Materials and Methods.

We found a correlation between the position of transport cargo and the position of the GLFG domains. We only considered cargo labels that were within the NPC, including the exclusion zone and nucleoplasmic basket. When GLFG labels were located in the cytoplasm, the cargo was likewise located on the cytoplasmic side (Fig. 8A,B,A′,B′). We also did not find labelling associated with the nucleoplasmic part of the NPC when there was no GLFG labelling on the nucleoplasmic side (Fig. 8A,B,A′,B′). When the GLFGs were evenly distributed about the plane of the NPC, we found the cargo located at this central plane (Fig. 8C,D,C′,D′). When the GLFG labelling was oriented to the nucleoplasmic side, again, we found the cargo labelling within the same region (Fig. 8E,F,E′,F′).

One possible explanation is that as cargo moves from cytoplasmic to nucleoplasmic side, some GLFG domains move with them. We know that cargo was moving in the cytoplasmic-to-nucleoplasmic direction when it was frozen, randomly trapping cargoes at any possible position in their route. It is reasonable to suppose that an import cargo that is closer to the nucleoplasm has travelled in time further along its transport route through the NPC. We can therefore reasonably suggest that GLFG domains caught at the same time, in the same position could be moving with the cargo. Because GLFG domain position modelling suggested a loose coordination of GLFG domain movement we speculate that it is individual, or limited numbers, of GLFG domains that move during the movement of each transport complex. The fact that we often observe all of the GLFG labelling on the same side as cargo could be because the Nab2pNLS–GFP is expressed at a high level, so there is a resulting large volume of traffic in the nuclear direction.

Anti-GLFG labels Nup116p GLFG domains, but also recognises Nup100p, Nup57p and Nup49p. The C-terminus of Nup116p is fixed at the central channel periphery and previous studies (Rout et al., 2000) have shown that C-terminal tags on these nucleoporins all locate to similar positions, although Nup116p and Nup100p are cytoplasmically biased, whereas Nup57p and Nup49 are symmetrical. GLFG labelling, however, is more dispersed, extends away from the central plane and is variable between NPCs. Moreover, there is a correlation between the position of GLFG labelling with the position of import cargoes travelling through NPCs. This suggests that there is a correlation between the movement of import cargoes with the position of GLFG domains, suggesting that GLFG domains might move with import complexes. In one possible hypothesis, this could be achieved by conformational restructuring of intrinsically disordered GLFG domains upon interaction with the relevant karyopherin.

DISCUSSION

We aimed to determine GLFG domain organisation and how this is involved in transport. We show that cytoplasmic filaments delineate a dome-shaped structure that partially constrains GLFG domains. Protruding material creates an exclusion zone around the NPC cytoplasmic face restricting entry of small transport-inert proteins. It is not a barrier to NLS-baring proteins, which appear to transiently accumulate near the channel central plane. The C-terminal anchor of Nup116p is located in the central channel. In contrast, GLFG domains, although mostly concentrated close to the central channel, can stretch up to 80 nm in either direction. The position of GLFG domains varies between NPCs and they can be oriented towards the cytoplasm, nucleoplasm or symmetrically. Import cargoes, which move in the cytoplasmic-to-nuclear direction, colocalise with GLFG domains, whether they are cytoplasmic, symmetric or nucleoplasmic suggesting that GLFG domains and import complexes move together.

Yeast have cytoplasmic filaments (Fahrenkrog et al., 1998; Kiseleva et al., 2004), but lack Nup358, the major vertebrate filament protein (Walther et al., 2002). We show that yeast cytoplasmic filaments are organised into a basket-like arrangement. A similar organisation is induced by high concentrations of RanGTP in *Xenopus* oocytes (Goldberg et al., 2000).

We show that GLFG domains do not appear to be a constituent of the cytoplasmic filaments, but are contained inside the basket-like structure. Some GLFG domains extend beyond this. Domain-specific and epitope tag immunogold labelling of isolated *Xenopus* oocyte nuclear envelopes, has shown that, like Nup116p *in vivo* here, the anchor of Nup62 is located near the central plane, whereas the FG domain extends out (Schwarz-Herion et al., 2007). FG domains of Nup153 collapse when bound to importin β *in vitro* and in oocytes (Lim et al., 2007). This is supported by our observation that yeast GLFG domains can be compacted into the NPC or extended. Eisele et al. (Eisele et al., 2010) showed, using atomic force microscopy, that dense FG domain films (with a similar density to the channel) did not collapse in the presence of importin β, but less densely packed ones could (Lim et al., 2007). This is consistent with the suggestion that some GLFG domains are densely packed in the channel and hence might not undergo reversible collapse (Eisele et al., 2010), but others can exist in extended, but reversibly collapsible conformations (Lim et al., 2007).

We suggest there may be two populations of GLFG domains: one densely packed into the channel with limited dynamics (Eisele et al., 2010), the other extending in an unfolded conformation. Because in some NPCs all the GLFG labelling is packed into the central channel, there might be some exchange between the populations. The peripheral, extended GLFG domains could retract into the central channel. However, retraction is presumably reversible in order to re-establish extended domains. Because we can correlate the position of transport cargoes with the position of GLFG domains, previous conclusions that transport factors induce this reversible collapse are supported (Lim et al., 2007).

In vitro the Nup116p GLFG domain folds into a compact coil that is cohesive and could form a gel at high concentrations in the channel (Yamada et al., 2010). Our *in vivo* results support such an arrangement for the majority of GLFG domains, but also show that a proportion can be more extended and unfolded. Double labelling also suggests that unfolded GLFGs become compacted into the channel during the passage of an import complex, because we always observe cargoes colocalising with GLFG domains. Our evidence supports the hypothesis that this represents a subset of GLFG domains that can dynamically fold and unfold.

It could be that the majority of FG domains are folded into the central channel forming a hydrogel or entropic barrier, seen as the dense exclusion zone in our TEM images, constrained by the cytoplasmic filaments seen by feSEM. There might be a subset of extended GLFG domains acting as an entropic barrier to inert molecules and possibly acting to capture passing import factors. Upon karyopherin–cargo binding, folding might occur, dragging import complexes into the densely packed channel.

FeSEM and TEM suggest a model where eight cytoplasmic filaments act as a flexible partial container for FG domains. Gaps between filaments are important as they allow import and export complexes to enter or leave the channel. Gaps also allow GLFG domains to extend beyond the confines of the cytoplasmic basket-like structure. We speculate that this could be important to 'extend the reach' of the NPC to increase cargo capture efficiency, and to keep a region around the NPC opening clear of cytosolic material: the exclusion zone. A similar 'exclusion zone' is well established on the NPC nucleoplasmic side, which is clearly visible as breaks in the peripheral heterochromatin, presumed to be delineated by the basket. The similar exclusion zone on the cytoplasmic face was probably not recognised because of the lack of such dense surrounding material.

Studies using the pair correlation function method (Cardarelli and Gratton, 2010) have indicated that movement of transport complexes through the NPC is a two-phase process with a fast transport component and a slower diffusion-like component. In contrast, passive diffusion through the NPC appears to consist of a single smooth, slower component. These conclusions are consistent with our observations that diffusion of GFP through the exclusion zone and NPC channel is spatially random and evenly scattered from cytoplasmic to nucleoplasmic ends of the NPC. Conversely, actively transported cargo is almost never observed within the exclusion zone. However, such cargo must travel through it, leading us to conclude that transit of an import complex through the exclusion zone must be rapid. We also observe accumulation of GFP–NLS near the central plane, suggesting that movement through this region is slower, possibly similar to the diffusion of GFP alone (Cardarelli and Gratton, 2010).

In agreement with our double labelling, showing correlation between the movement of cargo with GLFG domains, Cardarelli et al. (Cardarelli et al., 2012), used fluorescence correlation spectroscopy to show that a C-terminal GFP tag on the FG domain of Nup153 moves in a similar way to karyopherins and cargo during active transport. We therefore suggest that karyopherin-mediated import may be a two-phase process (Fig. 8G–I). Here, we only have evidence for the GLFG domains we have studied. The karyopherin could bind to the extended GLFG domain, inducing a restructuring event, resulting in rapid movement through the exclusion zone. The exclusion zone could be like a region of a pond next to the bank that is too densely planted for a large fish to enter. The intrinsically disordered GLFG domain would be like a fishing line cast beyond this region, catching a fish and reeling it back through the densely planted region as it restructures. This would localise the import complex to the central plane, where it would then diffuse, randomly, through the densely packed GLFG domains in the central channel, the short distance to the nucleoplasmic basket. The hydrophobic interactions between the transport factor and FG domains are weak and transient so we would expect the transport complex to 'hop' from one FG domain to another stochastically. Assuming the structural order in at least some GLFG domains is dependent on this binding, the presence of the intact transport complex in the central channel would keep the GLFG domains compacted, explaining our observation that when cargo is centrally located, GLFG domains do not extend in either direction. RanGTP is thought to bind karyopherin β within the basket (Kutay et al., 1997), where the import complex dissociates. Upon dissociation of the complex, the nucleoplasmically oriented GLFGs would no longer bind to karyopherin β and GLFG domains could unfold, creating a less-dense environment for the cargo to diffuse into the nucleoplasm.

It has been shown, by single molecule imaging using single-point illumination edge-excitation microscopy (Ma and Yang, 2010), that karyopherin β is spatially located to defined regions from a distance of ~80 nm into the cytoplasm, to a distance of ~80 nm into the nucleoplasm from the NPC central plane. This correlates well with our observation of the maximum distance that GLFG labelling is from the central plane. The GLFG domain of Nup116p is 592-amino-acids long (Yamada et al., 2010). A single amino acid is 0.36 nm in length. Therefore a fully extended Nup116p GLFG domain could be up to 200 nm in length if in a linear conformation. Of course, polypeptides are never in such a conformation and when 'intrinsically disordered', occupy random or loose coils (Bernadó and Svergun, 2012). Our measurements of the extent of the distance between the anchor and some GLFG domains gives the first indication that these proteins can adopt highly disordered states in the context of a cell, but mostly are folded into the NPC channel, which is more consistent with a collapsed coil (Yamada et al., 2010).

The nature of intrinsically disordered protein domains (Uversky, 2013) is controversial or even disputed *in vivo* (Janin and Sternberg, 2013). We can infer that some GLFG domains are disordered based on the distance between the anchor and GLFG domain, whereas others are more structured due to their closer proximity. We also infer some dynamic exchange between the two states due to the colocalisation of moving transport cargoes with GLFG domains. However, electron microscopy cannot directly give time-resolved information, other than snapshots, and therefore confirmation of these proposed dynamics will require further experiments using single-molecule light approaches.

Journal of Cell Science (2014) 127, 124–136 doi:10.1242/jcs.133272

Energetically, the proposed dynamics is not unreasonable. Intrinsically disordered domains have relatively flat 'energy landscapes' and can adopt multiple conformations with similar minimum energies (Uversky, 2013). Binding to a partner spontaneously stabilises limited or single conformation(s). Therefore there is no 'energy cost' to the cell in the initial binding and folding event. The cost comes in the dissociation and release of the import complex by Ran, which hydrolyses its GTP.

These results constitute further ultrastructural evidence, supporting previous live single-molecule imaging, that nuclear import is a two-phase process, with rapid entry through an entropic barrier, seen as the exclusion zone, driven by reversible collapse of GLFG domains, followed by a slower diffusion rate phase through the central channel, which is densely packed with FG domains. The non-random distribution of import cargo within the channel (Fiserova et al., 2010; Ma and Yang, 2010; Beck et al., 2007), towards the edge, suggests that although movement is at diffusion rates, it is spatially constrained, consistent with the FG domain organisation suggested in the Forest model (Yamada et al., 2010).

MATERIALS AND METHODS

Plasmids and yeast strains

We used yeast strains SWY 2285, SWY3603, SWY3292 and SWY3410 (Strawn et al., 2004). Additional, strains were obtained from the GFP-tag collection (Huh et al., 2003) and the TAP tag collection (Ghaemmaghami et al., 2003) and from Michael Rout (The Rockefeller University, New York, NY; Rout et al., 2000). Yeast were grown in YPD (1% yeast extract, 2% peptone, 2% glucose). Vectors used were: pNS167, pGFP-N-fus, *NAB2* NLS-GFP, *NAB2* NLS fused to GFP (Shulga et al., 2000), GFP-pESC-URA, pESC-URA, GFP.

Preparation of yeast nuclei for feSEM

Log-phase cells were washed (0.1 M Tris-HCl, 10 mM DTT pH 7.4, then 1.2 M Sorbitol, 20 mM potassium phosphate, 0.5 mM $MgCl_2$ pH 7.4), incubated with 150 µl Lyticase, 0.1% PEPA, 0.1% PMSF in 1.2 M Sorbitol, 20 mM potassium phosphate, 0.5 mM $MgCl_2$ pH 7.4 for ~35 minutes), lysed (by dilution 1:1 in 0.5 mM $MgCl_2$), attached to silicon chips and fixed by centrifugation through 4% paraformaldehyde, 0.5 mM $MgCl_2$, 0.2 M sucrose, in 20 mM potassium phosphate pH 6.5 (Kiseleva et al., 2007). Salt wash was omitted. Chemicals were obtained from Sigma-Aldrich, St. Louis, MO, unless otherwise stated. Samples were dehydrated in ethanol and critical-point dried using a Bal-tec CPD 030 (BAL-TEC, Balzers, Switzerland), sputter coated with 1.5 nm of chromium in a Cressington 308R (Cressington Scientific Instruments Ltd, Watford, UK), then viewed at 30 kV in a Hitachi S-5200 feSEM.

High-pressure freezing and freeze substitution of yeast for TEM

Cells were frozen using a Leica EM PACT (Leica Microsystems, Wetzlar, Germany). For FS (Fiserova and Goldberg, 2010) samples were then placed on top of frozen fixative (0.2% uranyl acetate, 0.2% glutaraldehyde, 0.01% osmium tetroxide, 5% H_2O in acetone), and cryofixed and dehydrated using the Leica EM AFS freeze-substitution unit programmed as follows. T1: −90℃, 49 hours; S1: 5℃ per hour up to −25℃; T2: −25℃, 12 hours; S2: 0℃, 0 hours; T3: −25℃, 50 hours. When step S2 was finished, acetone washes were performed (2–15 minutes) and samples were infiltrated with Monostep Lowycril HM20 at −25℃ (Polysciences, Eppelheim, Germany). Resin polymerisation was initiated and proceeded as follows. T1: −25℃, 24 hours; S1: 5℃ per hour up to 25℃; T2: 25℃, 24–100 hours. Blocks were trimmed and 60-nm sections cut.

Immunogold labelling for TEM and feSEM

Procedures were according to Fiserova and Goldberg (Fiserova and Goldberg, 2010). Sections attached to Formvar nickel grids, rinsed with three 1-minute washes of 0.1% glycine in PBS, blocked by four 1-minute washes of 1% BSA, PBS, and incubated with primary antibody for 1 hour, room temperature, then rinsed by four 2-minute washes of PBS. Secondary anti-rabbit-Ig antibody with 5-nm colloidal gold (Agar Scientific, Stansted, UK) was applied for 1 hour. Grids were rinsed three times in PBS for 5 seconds each, washed four times in PBS for 2 minutes and ten times in distilled water for 1 minute, then were placed in 1% uranyl acetate for 10 minutes and Reynold's lead citrate for 10 minutes. Grids were dried and observed at 120 kV with a Hitachi H-7600 TEM. Primary antibodies were rabbit polyclonal anti-GFP (Abcam, Cambridge, UK), affinity purified rabbit polyclonal antibody against GLFG domains (anti-GLFG) (WU956; Bucci and Wente, 1998), and affinity purified rabbit polyclonal antibody against the C-terminus of Nup116p (WU600; Bucci and Wente, 1998). For double labelling the same procedure was followed except primary antibodies were mixed, as were secondary antibodies at appropriate steps. Secondary antibodies were goat anti-rabbit-Ig conjugated to 1.4 nm Nanogold® (Nanoprobes.com) mixed with goat anti-mouse-Ig conjugated to 10 nm gold (Agar Scientific, Stansted, UK). The size of gold was enhanced with GoldEnhance™ EM (Nanoprobes.com) according to manufacturer's instructions. For immuno-feSEM (Goldberg and Fiserova, 2010), nuclei were prepared as above, fixed in 4% paraformaldehyde, 0.5 mM $MgCl_2$, 0.2 M sucrose, in 20 mM potassium phosphate pH 6.5, incubated with 1% glycine in PBS, washed, incubated with 1% BSA in PBS, then with primary antibody for 90 minutes, followed by two 10-minute washes, then the secondary-gold antibody for 1 hour and three further 10-minute washes with PBS, and fixation in 2% glutaraldehyde, 0.2% tannic acid, 0.5 mM $MgCl_2$, in 20 mM potassium phosphate pH 6.5.

Quantitative analysis

To aid in the analysis of TEM images, custom software (Delineator) was produced. The software implements a rapid workflow that uses human input to mark location, geometry and polarity of NPCs followed by an automated delineation algorithm to find gold particles. Measured positions are translated into a common coordinate system based on user-defined geometry. Manual inspection and correction of delineation is possible. The software was implemented using the cross-platform Python language, numarray numerical library and the wxPython GUI library.

Coordinate determination and nearest neighbour analysis of feSEM images was done in ImageJ, using an appropriate plugin (https://icme.hpc.msstate.edu/mediawiki/index.php/Nearest_Neighbor_Distances_Calculation_with_ImageJ#Author). Further morphometrical analysis was done using PAST (Hammer et al., 2001).

In analysis to determine the height of exclusion zone we wanted to check that height variation was not a sampling effect due to shape of the zone and position of the section. We looked at NPC sections that varied from ~40 nm to ~85 nm in width (which indicated where the section went through the NPC) in order to correlate NPC section width against exclusion zone height. We found there was no correlation (a calculated Pearson correlation coefficient of −0.03) indicating that position of section had little effect on measured height of exclusion zone and confirming that its height did indeed vary from NPC to NPC.

Modelling of GLFG domain locations

We described the distribution of particles across the 72 NPCs as follows. We assumed that the distribution of particles within each NPC followed a normal distribution with standard deviation, σ_w. We also assumed that the mean of the normal distribution varied between NPCs, and the mean associated with a NPC was also drawn from a normal distribution with mean μ and standard deviation σ_b. Finally, we assumed that σ_w was related to the NPC mean, $\bar{z}$ say), according to $\sigma_w=\beta_0+\beta_1\bar{z}+\beta_2\bar{z}^2$. This last assumption allowed us to look for evidence that the variation in the distribution of particles differed among NPCs, which might be expected if the structure of the NPC differed between the nucleus and the cytoplasm. Here, positive vertical locations indicate presence in the cytoplasm. Our model is described by five parameters: $\boldsymbol{\theta}=\{\mu, \sigma_b, \beta_0, \beta_1, \beta_2\}$ and the likelihood of the model, given the data, is

$$L(\boldsymbol{\theta})=\prod_{i=1}^{I}\int_{\bar{z}=-\infty}^{\infty} f(\bar{z}|\mu,\sigma_b)\prod_{j=1}^{J_i} f\left(z_{ij}\middle|\bar{z},\beta_0+\beta_1\bar{z}+\beta_2\bar{z}^2\right)d\bar{z}, \qquad (1)$$

where $I=72$, the number of NPCs, J_i is the number of particles in the i-th NPC sampled, and z_{ij} is the vertical location of the j-th particle sampled in NPC i.

We used likelihood ratio tests (LRTs) to see which form of our model best described our data. Specifically, we looked for evidence that the parameters μ, σ_b, β_1 and β_2 were non-zero. First, we looked for evidence of between NPC variation by comparing the two models having free parameters $\{\mu, \beta_0\}$ and $\{\mu, \sigma_b, \beta_0\}$. Next, we looked for evidence that the population mean, μ, was non-zero, and we then looked for evidence of either a linear or quadratic relation between the NPC mean and its standard deviation by comparing fits with β_1 and β_2 either fixed at zero or free. The test statistic for each LRT is $G=2(LL_1-LL_0)$, where LL_0 and LL_1 are the maximum log-likelihoods of the simpler and more complex model, respectively (i.e. the natural log of Eq. 1). If the data were generated by the simpler model, then G is approximately chi-square distributed with (k_1-k_0) degrees of freedom, where the k is the number of estimated model parameters.

SDS-PAGE and western blotting

Log-phase cells were pelleted at 2000 ***g*** for 10 minutes at 4℃, resuspended in 10 mM sodium azide, pelleted at 16,000 ***g*** for 1 minute, resuspended in SDS-PAGE sample buffer and vortexed for 2 minutes with glass beads. Glass beads were removed and samples stored at −20℃. Standard 10% SDS-PAGE gels were run (Prosieve®50, Lonza Rockland Inc.) and transferred overnight to PDVF membrane in standard Tris-glycine-ethanol buffer at 10 V. Membranes were blocked with 3% milk protein in PBS plus 0.1% Tween and incubated in the in the same buffer containing the anti-GLFG antibody at a 1:2500 dilution, washed three times with PBS-Tween, incubated with the horseradish-peroxidise-linked secondary antibody (donkey anti-rabbit-Ig, Abcam) in PBS/Tween, washed three times with PBS/Tween, and the bands were detected by chemiluminescence (Pierce ECL Plus, Thermo Scientific).

Image manipulation

Electron micrographs were optimised using Levels in Adobe Photoshop 7.0. TEM images in Figs 2, 3, 4, 7, 8 are presented as raw images (optimised contrast) on the left and interpreted image on right where membranes have been traced for clarity and gold particles are overlaid with a black dot. White dots in Fig. 5 were added in Adobe Photoshop to mark the position of gold particles on a simultaneously acquired backscatter image of same area (Goldberg and Fiserova, 2010). For western blots, individual lanes from the same or parallel blots were excised and aligned for appropriate comparisons, and brightness and/or contrast adjusted if necessary using Levels in Adobe Photoshop 7.0.

Acknowledgements

We thank Helen Grindley and Christine Richardson for technical support and data, Susan Wente and Becky Adams (Vanderbilt University, Nashville) for critical comments and yeast strains, plasmids and antibodies to Nup116p C-terminus and GLFG domain, and Michael Rout apart from the Protein-A-tagged Nup116p strain (The Rockefeller University, NY).

Competing interests

The authors declare no competing interests.

Author contributions

J.F., M.S. and M.W.G. contributed the experimental data, which was mostly analysed by J.F., M.S. and M.W.G. Image analysis software was developed by C.S. and modelling of G.L.F.G. domain locations was carried out by S.A.R. The project was conceived and supervised by M.W.G. with some experimental design from J.F. M.W.G. and J.F. prepared the manuscript, with intellectual input from all authors.

Funding

Work was supported by Biotechnology and Biological Sciences Research Council, UK [grant numbers BB/E015735/1 and BB/G011818/1 to M.G.].

Supplementary material

Supplementary material available online at
http://jcs.biologists.org/lookup/suppl/doi:10.1242/jcs.133272/-/DC1

References

Akey, C. W. and Radermacher, M. (1993). Architecture of the Xenopus nuclear pore complex revealed by three-dimensional cryo-electron microscopy. *J. Cell Biol.* **122**, 1-19.

Ban, N., Escobar, C., Garcia, R., Hasel, K., Day, J., Greenwood, A. and McPherson, A. (1994). Crystal structure of an idiotype-anti-idiotype Fab complex. *Proc. Natl. Acad. Sci. USA* **91**, 1604-1608.

Beck, M., Lucić, V., Förster, F., Baumeister, W. and Medalia, O. (2007). Snapshots of nuclear pore complexes in action captured by cryo-electron tomography. *Nature* **449**, 611-615.

Bernadó, P. and Svergun, D. I. (2012). Structural analysis of intrinsically disordered proteins by small-angle X-ray scattering. *Mol. Biosyst.* **8**, 151-167.

Bilokapic, S. and Schwartz, T. U. (2012). 3D ultrastructure of the nuclear pore complex. *Curr. Opin. Cell Biol.* **24**, 86-91.

Bucci, M. and Wente, S. R. (1998). A novel fluorescence-based genetic strategy identifies mutants of Saccharomyces cerevisiae defective for nuclear pore complex assembly. *Mol. Biol. Cell* **9**, 2439-2461.

Cardarelli, F. and Gratton, E. (2010). In vivo imaging of single-molecule translocation through nuclear pore complexes by pair correlation functions. *PLoS ONE* **5**, e10475.

Cardarelli, F., Lanzano, L. and Gratton, E. (2012). Capturing directed molecular motion in the nuclear pore complex of live cells. *Proc. Natl. Acad. Sci. USA* **109**, 9863-9868.

Cook, A., Bono, F., Jinek, M. and Conti, E. (2007). Structural biology of nucleocytoplasmic transport. *Annu. Rev. Biochem.* **76**, 647-671.

Denning, D. P., Patel, S. S., Uversky, V., Fink, A. L. and Rexach, M. (2003). Disorder in the nuclear pore complex: the FG repeat regions of nucleoporins are natively unfolded. *Proc. Natl. Acad. Sci. USA* **100**, 2450-2455.

Eisele, N. B., Frey, S., Piehler, J., Görlich, D. and Richter, R. P. (2010). Ultrathin nucleoporin phenylalanine-glycine repeat films and their interaction with nuclear transport receptors. *EMBO Rep.* **11**, 366-372.

Fahrenkrog, B., Hurt, E. C., Aebi, U. and Panté, N. (1998). Molecular architecture of the yeast nuclear pore complex: localization of Nsp1p subcomplexes. *J. Cell Biol.* **143**, 577-588.

Fernandez-Martinez, J. and Rout, M. P. (2012). A jumbo problem: mapping the structure and functions of the nuclear pore complex. *Curr. Opin. Cell Biol.* **24**, 92-99.

Fiserova, J. and Goldberg, M. W. (2010). Immunoelectron microscopy of cryofixed freeze-substituted Saccharomyces cerevisiae. *Methods Mol. Biol.* **657**, 191-204.

Fiserova, J., Richards, S. A., Wente, S. R. and Goldberg, M. W. (2010). Facilitated transport and diffusion take distinct spatial routes through the nuclear pore complex. *J. Cell Sci.* **123**, 2773-2780.

Ghaemmaghami, S., Huh, W. K., Bower, K., Howson, R. W., Belle, A., Dephoure, N., O'Shea, E. K. and Weissman, J. S. (2003). Global analysis of protein expression in yeast. *Nature* **425**, 737-741.

Goldberg, M. W. and Allen, T. D. (1992). High resolution scanning electron microscopy of the nuclear envelope: demonstration of a new, regular, fibrous lattice attached to the baskets of the nucleoplasmic face of the nuclear pores. *J. Cell Biol.* **119**, 1429-1440.

Goldberg, M. W. and Allen, T. D. (1995). Structural and functional organization of the nuclear envelope. *Curr. Opin. Cell Biol.* **7**, 301-309.

Goldberg, M. W. and Fiserova, J. (2010). Immunogold labelling for scanning electron microscopy. *Methods Mol. Biol.* **657**, 297-313.

Goldberg, M. W., Rutherford, S. A., Hughes, M., Cotter, L. A., Bagley, S., Kiseleva, E., Allen, T. D. and Clarke, P. R. (2000). Ran alters nuclear pore complex conformation. *J. Mol. Biol.* **300**, 519-529.

Hammer, Ø., Harper, D. A. T. and Ryan, P. D. (2001). PAST: Paleontological statistics software package for education and data analysis. *Palaeontol. Electronica* **4**, 4.

Ho, A. K., Shen, T. X., Ryan, K. J., Kiseleva, E., Levy, M. A., Allen, T. D. and Wente, S. R. (2000). Assembly and preferential localization of Nup116p on the cytoplasmic face of the nuclear pore complex by interaction with Nup82p. *Mol. Cell. Biol.* **20**, 5736-5748.

Hoelz, A., Debler, E. W. and Blobel, G. (2011). The structure of the nuclear pore complex. *Annu. Rev. Biochem.* **80**, 613-643.

Huh, W. K., Falvo, J. V., Gerke, L. C., Carroll, A. S., Howson, R. W., Weissman, J. S. and O'Shea, E. K. (2003). Global analysis of protein localization in budding yeast. *Nature* **425**, 686-691.

Iborra, F. J. and Cook, P. R. (1998). The size of sites containing SR proteins in human nuclei. Problems associated with characterizing small structures by immunogold labeling. *J. Histochem. Cytochem.* **46**, 985-992.

Janin, J. and Sternberg, M. J. E. (2013). Protein flexibility, not disorder, is intrinsic to molecular recognition. *F1000 Biol. Rep.* **5**, PMC3542771.

Kiseleva, E., Allen, T. D., Rutherford, S., Bucci, M., Wente, S. R. and Goldberg, M. W. (2004). Yeast nuclear pore complexes have a cytoplasmic ring and internal filaments. *J. Struct. Biol.* **145**, 272-288.

Kiseleva, E., Allen, T. D., Rutherford, S. A., Murray, S., Morozova, K., Gardiner, F., Goldberg, M. W. and Drummond, S. P. (2007). A protocol for isolation and visualization of yeast nuclei by scanning electron microscopy (SEM). *Nat. Protoc.* **2**, 1943-1953.

Kutay, U., Izaurralde, E., Bischoff, F. R., Mattaj, I. W. and Görlich, D. (1997). Dominant-negative mutants of importin-beta block multiple pathways of import and export through the nuclear pore complex. *EMBO J.* **16**, 1153-1163.

Lee, G. W., Melchior, F., Matunis, M. J., Mahajan, R., Tian, Q. and Anderson, P. (1998). Modification of Ran GTPase-activating protein by the small ubiquitin-related

modifier SUMO-1 requires Ubc9, an E2-type ubiquitin-conjugating enzyme homologue. *J. Biol. Chem.* **273**, 6503-6507.
Lim, R. Y., Fahrenkrog, B., Köser, J., Schwarz-Herion, K., Deng, J. and Aebi, U. (2007). Nanomechanical basis of selective gating by the nuclear pore complex. *Science* **318**, 640-643.
Ma, J. and Yang, W. (2010). Three-dimensional distribution of transient interactions in the nuclear pore complex obtained from single-molecule snapshots. *Proc. Natl. Acad. Sci. USA* **107**, 7305-7310.
Matunis, M. J., Wu, J. and Blobel, G. (1998). SUMO-1 modification and its role in targeting the Ran GTPase-activating protein, RanGAP1, to the nuclear pore complex. *J. Cell Biol.* **140**, 499-509.
Mohr, D., Frey, S., Fischer, T., Güttler, T. and Görlich, D. (2009). Characterisation of the passive permeability barrier of nuclear pore complexes. *EMBO J.* **28**, 2541-2553.
Murphy, R. M., Slayter, H., Schurtenberger, P., Chamberlin, R. A., Colton, C. K. and Yarmush, M. L. (1988). Size and structure of antigen-antibody complexes. Electron microscopy and light scattering studies. *Biophys. J.* **54**, 45-56.
Patel, S. S. and Rexach, M. F. (2008). Discovering novel interactions at the nuclear pore complex using bead halo: a rapid method for detecting molecular interactions of high and low affinity at equilibrium. *Mol. Cell. Proteomics* **7**, 121-131.
Patel, S. S., Belmont, B. J., Sante, J. M. and Rexach, M. F. (2007). Natively unfolded nucleoporins gate protein diffusion across the nuclear pore complex. *Cell* **129**, 83-96.
Rexach, M. and Blobel, G. (1995). Protein import into nuclei: association and dissociation reactions involving transport substrate, transport factors, and nucleoporins. *Cell* **83**, 683-692.
Ribbeck, K. and Görlich, D. (2001). Kinetic analysis of translocation through nuclear pore complexes. *EMBO J.* **20**, 1320-1330.
Rout, M. P., Aitchison, J. D., Suprapto, A., Hjertaas, K., Zhao, Y. and Chait, B. T. (2000). The yeast nuclear pore complex: composition, architecture, and transport mechanism. *J. Cell Biol.* **148**, 635-651.
Savas, J. N., Toyama, B. H., Xu, T., Yates, J. R., 3rd and Hetzer, M. W. (2012). Extremely long-lived nuclear pore proteins in the rat brain. *Science* **335**, 942.
Schwarz-Herion, K., Maco, B., Sauder, U. and Fahrenkrog, B. (2007). Domain topology of the p62 complex within the 3-D architecture of the nuclear pore complex. *J. Mol. Biol.* **370**, 796-806.
Shulga, N., Mosammaparast, N., Wozniak, R. and Goldfarb, D. S. (2000). Yeast nucleoporins involved in passive nuclear envelope permeability. *J. Cell Biol.* **149**, 1027-1038.
Strawn, L. A., Shen, T., Shulga, N., Goldfarb, D. S. and Wente, S. R. (2004). Minimal nuclear pore complexes define FG repeat domains essential for transport. *Nat. Cell Biol.* **6**, 197-206.
Uversky, V. N. (2013). Unusual biophysics of intrinsically disordered proteins. *Biochim. Biophys. Acta* **1834**, 932-951.
Wälde, S. and Kehlenbach, R. H. (2010). The Part and the Whole: functions of nucleoporins in nucleocytoplasmic transport. *Trends Cell Biol.* **20**, 461-469.
Walther, T. C., Pickersgill, H. S., Cordes, V. C., Goldberg, M. W., Allen, T. D., Mattaj, I. W. and Fornerod, M. (2002). The cytoplasmic filaments of the nuclear pore complex are dispensable for selective nuclear protein import. *J. Cell Biol.* **158**, 63-77.
Wu, J., Matunis, M. J., Kraemer, D., Blobel, G. and Coutavas, E. (1995). Nup358, a cytoplasmically exposed nucleoporin with peptide repeats, Ran-GTP binding sites, zinc fingers, a cyclophilin A homologous domain, and a leucine-rich region. *J. Biol. Chem.* **270**, 14209-14213.
Yamada, J., Phillips, J. L., Patel, S., Goldfien, G., Calestagne-Morelli, A., Huang, H., Reza, R., Acheson, J., Krishnan, V. V., Newsam, S. et al. (2010). A bimodal distribution of two distinct categories of intrinsically disordered structures with separate functions in FG nucleoporins. *Mol. Cell. Proteomics* **9**, 2205-2224.
Yang, Q., Rout, M. P. and Akey, C. W. (1998). Three-dimensional architecture of the isolated yeast nuclear pore complex: functional and evolutionary implications. *Mol. Cell* **1**, 223-234.
Zuleger, N., Kerr, A. R. and Schirmer, E. C. (2012). Many mechanisms, one entrance: membrane protein translocation into the nucleus. *Cell. Mol. Life Sci.* **69**, 2205-2216.

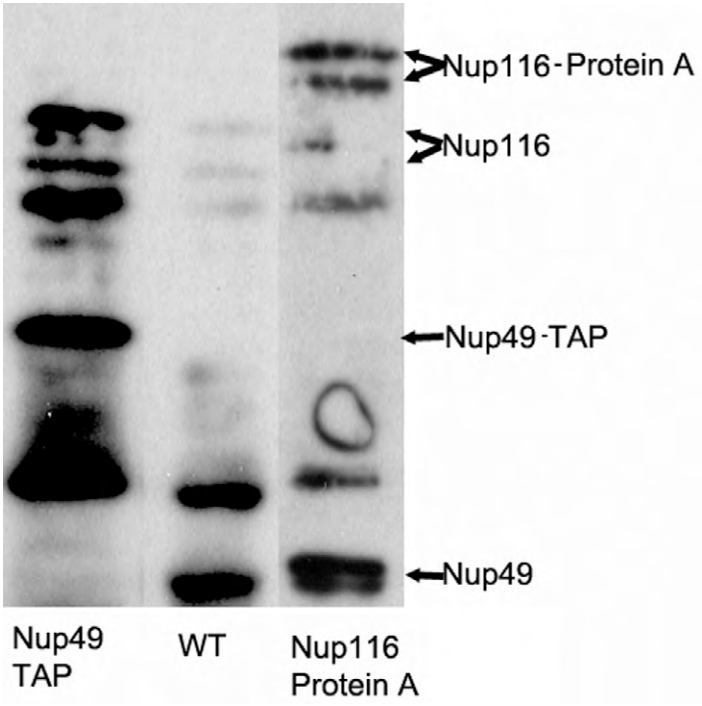

F**ig. S1.** Western blot using anti-GLFG antibody (WU956) showing the band shift of the ~49kD band when Nup49p is TAP tagged and of the ~120kD bands when Nup116p is fused to Protein A.